Vol 18 No 7, July 2009
1674-1056/2009/18(07)/2757-07

Chinese Physics B

© 2009 Chin. Phys. Soc.
and IOP Publishing Ltd

Investigation of composite electromagnetic scattering from ship-like target on the randomly rough sea surface using FDTD method*

Li Juan(李 娟)†, Guo Li-Xin(郭立新), Zeng Hao(曾 浩), and Han Xu-Biao(韩旭彪)

School of Science, Xidian University, Xi'an 710071, China

(Received 25 Dcember 2008; revised manuscript received 3 February 2009)

Composite electromagnetic scattering from a two-dimensional (2D) ship-like target on a one-dimensional sea surface is investigated by using the finite-difference time-domain (FDTD) method. A uniaxial perfectly matched layer is adopted for truncation of FDTD lattices. The FDTD updated equations can be used for the total computation domain by choosing the uniaxial parameters properly. To validate the proposed numerical technique, a 2D infinitely long cylinder over the sea surface is taken into account first. The variation of angular distribution of the scattering changing with incident angle is calculated. The results show good agreement with the conventional moment method. Finally, the influence of the incident angle, the polarization, and the size of the ship-like target on the composite scattering coefficient is discussed in detail.

Keywords: finite-difference time-domain, uniaxial perfectly matched layer, sea surface, electromagnetic scattering

PACC: 4120, 4110H

1. Introduction

In recent years, the composite electromagnetic scattering between the randomly rough surface and target has attracted considerable interest in the fields of radar surveillance, target tracking, oceanic remote sensing, etc. However, the study of such electromagnetic scattering models is a complex and difficult subject due to the complicated interactions between the target and underlying rough surface. Some methods have been used to deal with the problem. For example, the "four-path" method,[1] the image technique, and the multi-pole algorithm[2] have been investigated for a target above a flat surface. The reciprocity theorem[3,4] is adopted to study the electromagnetic scattering from the object above a one-dimensional slightly rough surface. The method of moments (MOM)[5] was employed to calculate the scattering of a target above a rough surface. The generalized forward–backward method, the multiple sweep method of Moments,[6] and the hybrid method[7] were analysed for the electromagnetic scattering from target located above an ocean-like rough surface.

In this paper, the finite-difference time-domain (FDTD) algorithm is utilized to study the composite electromagnetic scattering from a two-dimensional (2D) ship-like target floating on a rough sea surface. In our previous work, the FDTD method was used to analyse the scattering from a target above a rough surface.[8,9] The uniaxial perfectly matched layer (UPML) medium is placed at the outer extremities of the mesh in the paper. In the uniaxial medium the finite-difference equations are suitable for all the computation domain due to the field-satisfying Maxwell's equations, which makes the algorithm convenient and accordant in use. By comparing the FDTD algorithm with other numerical methods, there are some advantages: the rough surface and target may be a perfect electrical conductor (PEC) and dielectric, due to the fact that no other changes need to be done in the original FDTD code except the part where the material constants are set in each cell. In addition, the results obtained by this method are in the time domain, and can indicate both the transient behavior as well as the steady state. This paper is arranged as follows: the theoretical formulae for calculating a composite scattering field by FDTD are developed in Section 2. Numerical results of the compos-

*Project supported by the National Natural Science Foundation of China (Grant No 60571058), the Specialized Research Fund for the Doctoral Program of Higher Education, China (Grant No 20070701010).

†E-mail: lijuan029@yeah.net

ite scattering between a 2D ship-like target and the underlying sea surface under different conditions are presented and discussed in Section 3, which include the incident angle, polarization, and the size of 2D ship-like target. Section 4 gives the conclusion and the further investigation in this topic.

2. FDTD method in the scattering model

A one-dimensional random sea surface profile with PM spectrum is simulated by the Monte Carlo method.[10] It is assumed that the length of sea surface is L, the number of the point discretized at equal intervals is $M+1$, and the distance of two adjacent points is Δx, where $L = M \cdot \Delta x$. And the altitude of every point $x_m = m\Delta x\,(m = 1, \ldots, M)$ on the sea surface is defined as

$$\zeta(x_m, t) = \frac{1}{L} \sum_{i=-M/2}^{M/2-1} F(k_i) \mathrm{e}^{-\mathrm{j}k_i x_m} \tag{1}$$

where, for $i \geq 0$

$$F(k_i) = [2\pi L W(k_i)]^{1/2} \times \begin{cases} [N(0,1) + \mathrm{j}N(0,1)]/\sqrt{2} & i \neq 0, M/2; \\ N(0,1). & i = 0, M/2, \end{cases} \tag{2}$$

For $i < 0$, $F(k_i) = F(k_{-i})^*$, where the asterisk implies complex conjugate. $N(0,1)$ is a random variant with a Gaussian distribution of zero mean and unit variance. $k_i = 2\pi i/L$, and $W(k_i)$ is the Pierson–Moskowitz ocean power spectrum function[11] i.e.

$$W(k_i) = \begin{cases} \dfrac{\alpha}{4|k_i|^3} \exp\left(-\dfrac{\beta g^2}{k_i^2 U_{19.5}^4} \right) & k_i \geq 0; \\ 0 & k_i < 0, \end{cases} \tag{3}$$

where $\alpha = 8.10 \times 10^{-3}$ and $\beta = 0.74$ are empirical constants, g is the gravitational acceleration equal to $9.81\mathrm{m/s}^2$, $U_{19.5}$ represents wind speed in meters per second measured at a height of 19.5 m above the sea surface, and k_i is the spatial frequency in the x direction. Usually Eq.(1) is treated with a fast Fourier transform.

It is important to know the division of computation region with FDTD algorithm in calculating composite scattering from a ship-like target above the sea surface. The incident wave is generated on the connective boundary (see Fig.1), and the UPML absorbing medium is the outer boundary of FDTD region. In addition, the output boundary must be set by making a near-to-far transformation to obtain the far fields. In what follows, the three boundaries will be investigated.

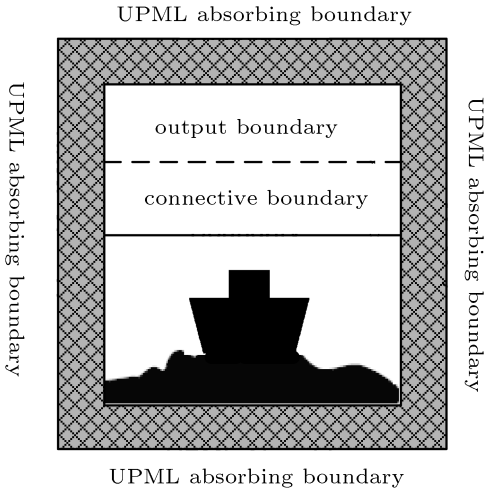


Fig.1. Division model of the computation region for the FDTD algorithm.

In theory, the computation domain should be unbounded for the scattered field existing in infinite free space. But no computer can store an unlimited amount of data. To deal with the conflict, a virtual absorbing boundary (see Fig.1) must be built, and the outgoing waves have to propagate outward without non-physical reflection from the boundary. There are many developments in absorbing boundary condition to implement the FDTD method, where the UPML absorbing media[12,13] are used to terminate the FDTD lattices, in which the finite-difference equations can be used for the total computation domain due to the fields satisfying Maxwell's equations (Ampere's and Faraday's laws). This makes the algorithm efficient since one does not have to take special care of the interface plane between the boundary and the interior regions. In addition, the uniaxial medium can be perfectly matched to an interior lossy medium without any modification except for properly choosing the uniaxial parameters. For the 2D Maxwell's equations, only E_z-, H_x-, H_y- field components(TM case)/H_z-, E_x-, E_y- field components (TE case) are nonzero. In the uniaxial medium, Faraday's law

for TM wave is expressed as

$$\frac{\partial E_z}{\partial y} = -\mathrm{j}w\mu_1 \frac{s_y}{s_x} H_x,$$
$$\frac{\partial E_z}{\partial x} = \mathrm{j}w\mu_1 \frac{s_x}{s_y} H_y. \tag{4}$$

And the Ampere's law is

$$\frac{\partial H_y}{\partial x} - \frac{\partial H_x}{\partial y} = (\mathrm{j}w\varepsilon_1 + \sigma_1) s_x s_y E_z, \tag{5}$$

where, $\mathrm{j} = \sqrt{1}$, w is the angular frequency, ε_1, μ_1 and σ_1 represent the parameters of interior medium. s_x and s_y are only spatially variant along the x and y directions, and $s_x = k_x + \sigma_x/\mathrm{j}w\varepsilon_0$, $s_y = k_y + \sigma_y/\mathrm{j}w\varepsilon_0$, referring to Ref.[12]. In Eq.(4), the intermediate variables B_x and B_y are introduced as

$$B_x = \frac{\mu_1}{s_x} H_x, \quad B_y = \frac{\mu_1}{s_y} H_y. \tag{6}$$

And in Eq.(5), the intermediate variables P'_z and P_z are given by

$$P'_z = s_y s_x E_z, \quad P_z = P'_z / s_x. \tag{7}$$

Using a Fourier transform where $\mathrm{j}w \to \partial/\partial t$, can transform Faraday's law into the time domain. Thus, the magnetic fields are obtained by the following relations $E_z \to B_x$, $B_y \to H_x$, H_y

$$\frac{\partial E_z}{\partial y} = -k_y \frac{\partial B_x}{\partial t} - \frac{\sigma_y}{\varepsilon_0} B_x, \tag{8a}$$

$$k_x \frac{\partial B_x}{\partial t} + \frac{\sigma_x}{\varepsilon_0} B_x = \mu_1 \frac{\partial H_x}{\partial t}; \tag{8b}$$

$$\frac{\partial E_z}{\partial x} = k_x \frac{\partial B_y}{\partial t} + \frac{\sigma_x}{\varepsilon_0} B_y, \tag{9a}$$

$$k_y \frac{\partial B_y}{\partial t} + \frac{\sigma_y}{\varepsilon_0} B_y = \mu_1 \frac{\partial H_y}{\partial t}. \tag{9b}$$

Similarly, for Ampere's law the electric field is deduced by the relations H_x, $H_y \to P'_z \to P_z \to E_z$,

$$\frac{\partial H_y}{\partial x} - \frac{\partial H_x}{\partial y} = \varepsilon_1 \frac{\partial P'_z}{\partial t} + \sigma_1 P'_z, \tag{10a}$$

$$\frac{\partial P'_z}{\partial t} = k_x \frac{\partial P_z}{\partial t} + \frac{\sigma_x}{\varepsilon_0} P_z, \tag{10b}$$

$$\frac{\partial P_z}{\partial t} = k_y \frac{\partial E_z}{\partial t} + \frac{\sigma_y}{\varepsilon_0} E_z. \tag{10c}$$

Using central difference approximation, the difference expressions of Eqs.(8–10) are as follows:

$$B_x^{n+\frac{1}{2}}\left(i, j+\frac{1}{2}\right) = \frac{\frac{k_y(m)}{\Delta t} - \frac{\sigma_y(m)}{2\varepsilon_0}}{\frac{k_y(m)}{\Delta t} + \frac{\sigma_y(m)}{2\varepsilon_0}} \cdot B_x^{n-\frac{1}{2}}\left(i, j+\frac{1}{2}\right) - \frac{\frac{1}{\Delta y}}{\frac{k_y(m)}{\Delta t} + \frac{\sigma_y(m)}{2\varepsilon_0}} \cdot \left(E_z^n(i, j+1) - E_z^n(i, j)\right), \tag{11}$$

$$H_x^{n+\frac{1}{2}}\left(i, j+\frac{1}{2}\right) = H_x^{n-\frac{1}{2}}\left(i, j+\frac{1}{2}\right) + \frac{\frac{k_x(m)}{\Delta t} + \frac{\sigma_x(m)}{2\varepsilon_0}}{\mu_1/\Delta t} \cdot B_x^{n+\frac{1}{2}}\left(i, j+\frac{1}{2}\right) - \frac{\frac{k_x(m)}{\Delta t} - \frac{\sigma_x(m)}{2\varepsilon_0}}{\mu_1/\Delta t} \cdot B_x^{n-\frac{1}{2}}\left(i, j+\frac{1}{2}\right), \tag{12}$$

$$B_y^{n+\frac{1}{2}}\left(i+\frac{1}{2}, j\right) = \frac{\frac{k_x(m)}{\Delta t} - \frac{\sigma_x(m)}{2\varepsilon_0}}{\frac{k_x(m)}{\Delta t} + \frac{\sigma_x(m)}{2\varepsilon_0}} \cdot B_y^{n-\frac{1}{2}}\left(i+\frac{1}{2}, j\right) + \frac{\frac{1}{\Delta x}}{\frac{k_x(m)}{\Delta t} + \frac{\sigma_x(m)}{2\varepsilon_0}} \cdot \left(E_z^n(i+1, j) - E_z^n(i, j)\right), \tag{13}$$

$$H_y^{n+\frac{1}{2}}\left(i+\frac{1}{2}, j\right) = H_y^{n-\frac{1}{2}}\left(i+\frac{1}{2}, j\right) + \frac{\frac{k_y(m)}{\Delta t} + \frac{\sigma_y(m)}{2\varepsilon_0}}{\mu_1/\Delta t} \cdot B_y^{n+\frac{1}{2}}\left(i+\frac{1}{2}, j\right) - \frac{\frac{k_y(m)}{\Delta t} - \frac{\sigma_y(m)}{2\varepsilon_0}}{\mu_1/\Delta t} \cdot B_y^{n-\frac{1}{2}}\left(i+\frac{1}{2}, j\right), \tag{14}$$

$$\begin{aligned} {P'}_z^{n+1}(i,j) = {} & \frac{\varepsilon_1(m)/\Delta t - 0.5\cdot\sigma_1(m)}{\varepsilon_1(m)/\Delta t + 0.5\cdot\sigma_1(m)} \cdot {P'}_z^{n}(i,j) + \frac{1}{\varepsilon_1(m)/\Delta t + 0.5\cdot\sigma_1(m)} \\ & \times \left[\frac{1}{\Delta x} \cdot \left(H_y^{n+\frac{1}{2}}\left(i+\frac{1}{2}, j\right) - H_y^{n+\frac{1}{2}}\left(i-\frac{1}{2}, j\right)\right)\right. \\ & \left. - \frac{1}{\Delta y} \cdot \left(H_x^{n+\frac{1}{2}}\left(i, j+\frac{1}{2}\right) - H_x^{n+\frac{1}{2}}\left(i, j-\frac{1}{2}\right)\right)\right], \end{aligned} \tag{15}$$

$$P_z^{n+1}(i,j) = \frac{k_x(m)/\Delta t - \sigma_x(m)/(2\varepsilon_0)}{k_x(m)/\Delta t + \sigma_x(m)/(2\varepsilon_0)} P_z^n(i,j) + \frac{1/\Delta t}{k_x(m)/\Delta t + \sigma_x(m)/(2\varepsilon_0)} \left[{P'}_z^{n+1}(i,j) - {P'}_z^{n}(i,j)\right], \tag{16}$$

$$E_z^{n+1}(i,j) = \frac{k_y(m)/\Delta t - \sigma_y(m)/(2\varepsilon_0)}{k_y(m)/\Delta t + \sigma_y(m)/(2\varepsilon_0)} E_z^n(i,j) + \frac{1/\Delta t}{k_y(m)/\Delta t + \sigma_y(m)/(2\varepsilon_0)} \left(P_z^{n+1}(i,j) - P_z^n(i,j)\right), \tag{17}$$

where i and j denote the grid points along x and y directions, respectively, and the superscript n is the number of time step; m denotes $(i, j+1/2)$ in Eqs.(11) and (12); it denotes $(i+1/2, j)$ in Eqs.(13) and (14), and (i, j) in Eqs.(15)–(17); Δx and Δy are respectively the spatial increments in the x- and y-directions, and Δt is the time increment. To ensure the stability and accuracy[14] of FDTD algorithm, in this paper the spatial increment and temporal increment could be set to $\Delta x = \Delta y = \delta = \lambda/20$, $\Delta t = 0.5 \times \delta/c$, and c is the light speed in vacuum. The finite-difference equations for the TE wave[15] can be obtained by similar transformations, which are not given here.

In Fig.2, a plane wave of unit amplitude $\boldsymbol{E}_{\mathrm{i}} = \hat{\boldsymbol{z}} \exp(-\mathrm{j}(\boldsymbol{k} \cdot \boldsymbol{r} + wt))$ propagates in the direction of θ_{i} relative to the y-axis, θ_{i} being the incident angle. Let the propagation direction $\boldsymbol{k}$ be the y'-axis, direction $\boldsymbol{E}_{\mathrm{i}}$ the z'-axis, and build the rectangular

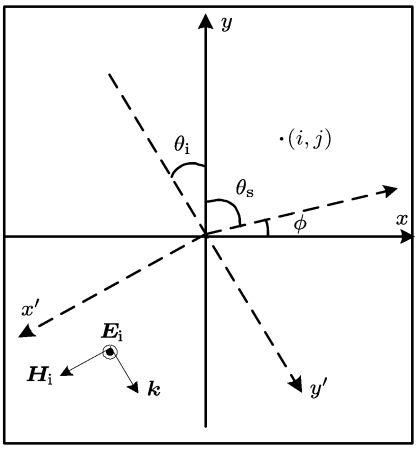


Fig.2. Projection of the node on the connective boundary onto the y'-axis.

coordinate $x'y'z'$. In the FDTD algorithm, the connective boundary can divide the computation region into the total field region and the scattered field region. But the incident electrical field $\boldsymbol{E}_{\mathrm{i}}$ and magnetic field $\boldsymbol{H}_{\mathrm{i}}$ only exist in the total field region. To solve the problem, the incident field is generated on the connective boundary by the equivalent theory.[8,9] In numerical implementations of composite scattering, finite-length rough surface must be used to model scattering from infinite surface. When a plane wave strikes the finite-length rough surface, boundary reflection occurs. One way of minimizing reflection is to construct an incident wave that tapers to very small values at the surface edges. Reflection still occurs, but it makes negligible contributions to the scattered field. To solve this problem, Fung[16] put forward the Gaussian window function to guard against the truncation effect. And the Gaussian window function is expressed as

$$G(x,y) = \exp\left\{ -\left[(x-x_0)^2 + (y-y_0)^2 \right] \left(\frac{\cos\theta_i}{T} \right)^2 \right\}, \quad (18)$$

where x_0 and y_0 are the spatial coordinates at the centre of the connective boundary. T is a constant which determines the width of the window function, $\cos\theta_i/T = 2.6/\rho_{\mathrm{m}}$ and ρ_{m} is the minimum distance from the centre (x_0, y_0) to the surface edge.

The near fields for the composite model of 2D ship-like target and underlying sea surface can be obtained on the basis of theory described above. As indicated in Ref.[15], a way to obtain the far fields is to do a near-to-far field transformation, which is based on the surface equivalence theorem. The transform formula for the output boundary is expressed as

$$\boldsymbol{E}_{\mathrm{s}} = \hat{\boldsymbol{z}} \frac{1}{2} \sqrt{\frac{\mathrm{j}k}{2\pi r}} \exp(-\mathrm{j}kr) \left(-z f_z - f_{mx} \sin\phi\right), \quad (19)$$

where $\mathrm{j} = \sqrt{-1}$ and k is the incident wave number, $k = |\boldsymbol{k}|$; r is the distance from the origin in the reference coordinates to any point at infinity, and z is the wave impedance. ϕ represents the angle between the direction of scattered field and x-axis, with $\phi = 90^\circ - \theta_{\mathrm{s}}$, θ_{s} being the scattered angle (as shown in Fig.2); f_z and f_{mx} are the terms which are related to the equivalent surface electric and magnetic currents written as

$$f_z = -\Delta x \sum_i H_x \left(i, j+\frac{1}{2} \right) \times \exp\left(\mathrm{j}k_0 \left(\left(j+\frac{1}{2} \right) \sin\phi \Delta y + i \cos\phi \Delta x \right) \right), \quad (20)$$

$$f_{\mathrm{mx}} = -\Delta x \sum_i E_z(i,j) \exp(\mathrm{j}k_0 (j \sin\phi \Delta y + i \cos\phi \Delta x)). \quad (21)$$

Substituting Eqs.(20), (21) into Eq.(19), the far-zone scattered field $\boldsymbol{E}_{\mathrm{s}}$ can be acquired, and the radar scattering coefficient[17] in the far-zone is defined as

$$\sigma = \lim_{r\to\infty} \frac{2\pi r}{L} \frac{|\boldsymbol{E}_{\mathrm{s}}|^2}{|\boldsymbol{E}_{\mathrm{i}}|^2}. \quad (22)$$

3. Numerical results and discussions

In order to ensure the validity of FDTD algorithm presented in the paper, in Fig.3 we firstly compute the angular distribution of bistatic scattering coefficient from a PEC cylinder with radius λ and altitude of $h = 3\lambda$ above a sea surface 180λ in length using the conventional MOM[18] and FDTD algorithm, respectively. In Fig.3 the UPML thickness is 5δ, the TM-polarized incidence wave is considered, the wind speed is 3 m/s, and incident frequency 0.3 GHz. It is obvious that the angular distribution of scattering coefficient for both incident angles 30° (Fig.3(a)) and 60° (Fig.3(b)) obtained by FDTD algorithm is in good agreement with that obtained by MOM over the whole scattered angular range, which demonstrates the effectiveness and accuracy of FDTD algorithm.

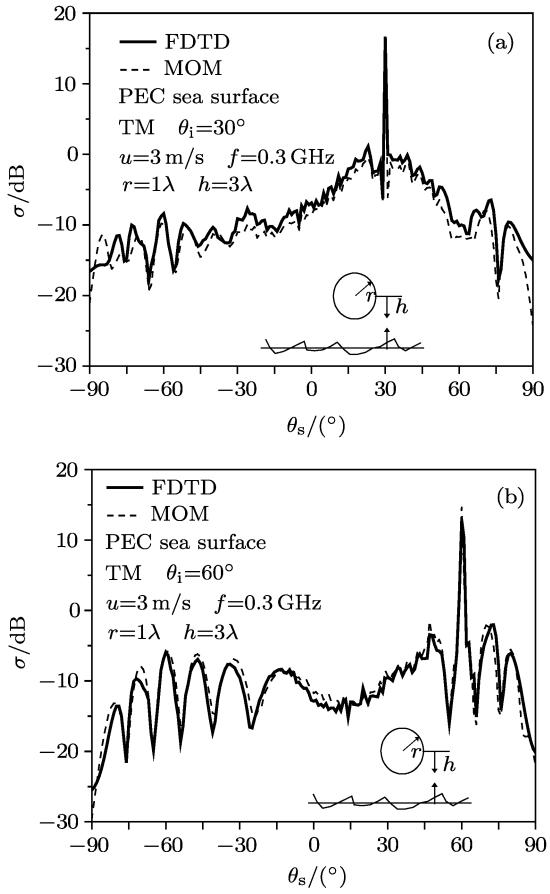


Fig.3. Comparison of the two different methods for bistatic scattering coefficient σ for a PEC cylinder above the PEC rough sea surface.

In what follows, the numerical results of composite scattering from a 2D ship-like target and a rough sea surface are presented and analysed in detail. The geometry of the 2D ship model is shown in Fig.4, where h represents the distance from the bottom of the ship to the sea surface, and the size of ship is determined by the parameter l. In performing the calculation, the size of the sea surface is $L = 260\lambda$, the incident frequency 1.0 GHz, the relative dielectric constant of sea water[19] is $\varepsilon_r = (72.0, 84.0)$, and the randomly rough sea surface is created by 45 Monte Carlo realizations.

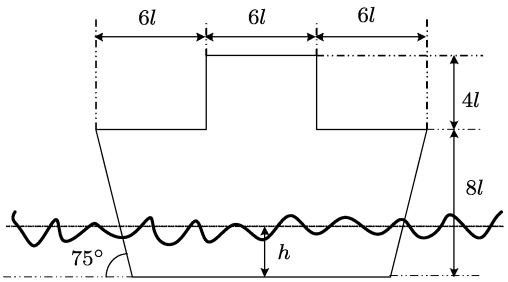


Fig.4. Geometry of 2D ship-like target.

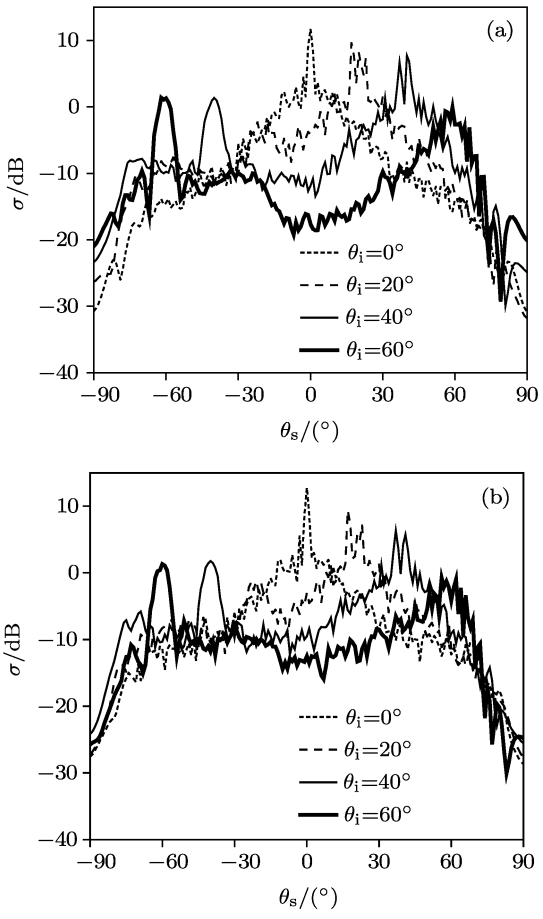


Fig.5. Bistatic scattering coefficient for different incident angles $l = 1.5\lambda$ and $h = 4.5\lambda$ (a) TM, (b) TE.

The dependence of the angular distribution of scattering coefficient for a 2D ship-like target located

above a dielectric sea surface on the incident angle is depicted in Fig.5, where the wind speed $U_{19.5} = 3$ m/s is considered. The parameters of 2D ship-like target is $l = 1.5\lambda$ and $h = 4.5\lambda$. It can be observed easily that for the incident angle $\theta_i = 0°$ the scattering coefficient in the specular direction has a more prominent peak and with the increase of incident angle the peak becomes ambiguous for both TM-polarized (Fig.5(a)) and TE-polarized incidence (Fig.5(b)). In addition, it is easily found that as the incident angle increases to 40°, an obvious peak occurs in the backward direction.

To further explore the important scattering characteristics of the ship–sea surface, in Fig.6, the effect of the size of the ship-like target on the composite scattering coefficient is analysed for the wind speed $U_{19.5} = 3$ m/s (Fig.6(a)) and $U_{19.5} = 5$ m/s (Fig.6(b)), where the TM polarization is investigated. It is shown that the bistatic scattering coefficient near the specular direction decreases with the increase of the size of the ship-like target (except for the specular direction). Another point worth noting is that the larger the ship size, the more obvious the peak in the backward direction is observed.

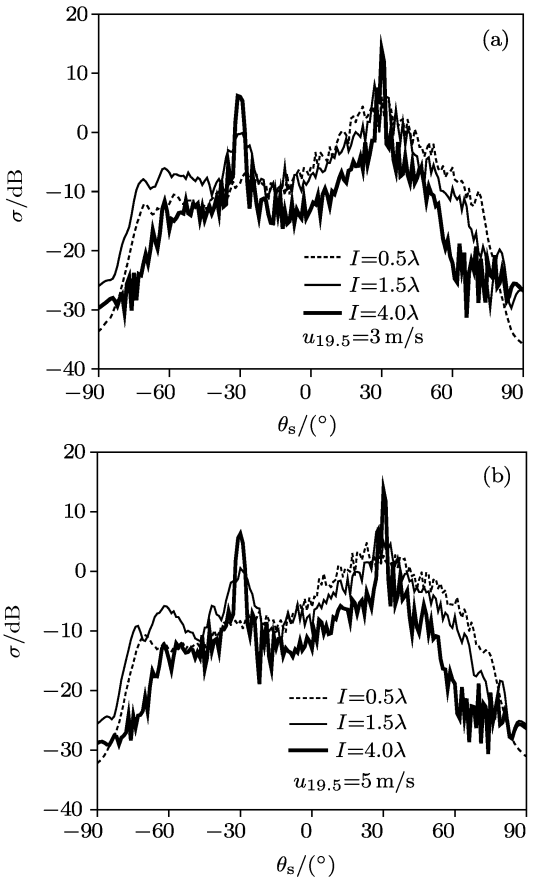


Fig.6. Bistatic scattering coefficient for different size of ship-like target $\theta_i = 30°$ and $h = 2.0\lambda$. (a) $U_{19.5} = 3$ m/s, (b) $U_{19.5} = 5$ m/s.

In addition, the effect of the wind speed $U_{19.5}$ and the depth h of the ship-like target immersing in sea water on the composite scattering coefficient is also investigated in our work. It can be found that the changes of the composite scattering coefficient are 'not sensitive' to the wind speed $U_{19.5}$ and the depth h.

4. Conclusions

This paper presents a study of composite electromagnetic scattering from a 2D ship-like target floating on a rough sea surface by using a FDTD algorithm. The basic theory of the FDTD method for calculating the composite scattered field is presented, including the generation of incident wave, the UPML under absorbing boundary condition, and a transform from near- to far-field on the output boundary. The bistatic scattering coefficient from the cylinder above a randomly rough sea surface by using the present method is compared with the numerical results obtained by the conventional Method of Moment, which verifies the effectiveness and accuracy of the FDTD algorithm. Finally, the dependence of the angular distribution of bistatic scattering coefficient on the incident angle, the polarization and the size of ship are investigated and analysed in detail. Future investigation will be on the composite electromagnetic scattering from a 3D ship model above a 2D rough sea surface, which is more important for practical application.

References

[1] Johnson J T 2001 *Microw. Opt. Techn. Lett.* **30** 130

[2] Li L, He J Q, Liu Z J and Carin L 2003 *IEEE Trans. Antennas Propag.* **51** 810

[3] Wang Y H, Guo L X and Wu Q 2006 *Chin. Phys.* **15** 1755

[4] Guo L X and Kim C Y 2002 *Microw. Opt. Techn. Let.* **33** 142

[5] Wang X, Wang C F , Gan Y B and Li L W 2003 *Progress in Electromagnetics Research, PIER* **40** 207

[6] Colak D, Burkhold R J and Newman E H 2007 *Microw. Opt. Techn. Let.* **49** 243

[7] Wang R, Guo L X, Qin S T and Wu Z S 2008 *Acta Phys. Sin.* **57** 3473 (in Chinese)

[8] Li J , Guo L X and Zeng H 2008 *Waves in Random and Complex Media* **18** 641

[9] Li J , Guo L X and Zeng H 2008 *Progress in Electromagnetics Research, PIER* **88** 197

[10] Kuga Y and Phu P 1996 *Progress in Electromagnetics Research, PIER* **14** 37

[11] Toporkov J V and Brown G S 2001 *IEEE Trans. Geosci. Remote Sensing* **38** 1616

[12] Gedney S D 1996 *IEEE Trans. Antennas Propagal.* **44** 1630

[13] Gedney S D 1996 *Electromagnetics* **16** 425

[14] Juntunen J S and Tsiboukis T D 2000 *IEEE Trans. on Microwave Theory Tech.* **48** 582

[15] Taflove A and Hagness S C 2005 *Computational Electrodynamics: The Finite-Difference Time-Domain Method* (Norwood, MA: Artech House)

[16] Fung A K 1994 *IEEE Trans. Geosci. Remote Sensing* **32** 986

[17] Ruck G, Barrick D E, Stuart W D and Krichbaum C K 1970 *Radar Cross Section Handbook* (New York: Plenum Press)

[18] Tsang L, Kong J A and Ding K H 2001 *Scattering of Electromagnetic Wave* (USA: John Wiley & Sons. Inc)

[19] Ulaby F T 1982 *Microwave Remote Sensing* (London: Addison-Wesley)